

Improved neutral and plasma density control with increasing lithium wall coatings in the Lithium Tokamak Experiment- β (LTX- β)

A. Maan^{a,*}, D.P. Boyle^a, R. Majeski^a, S. Banerjee^a, M. Francisquez^a, R. Kaita^a, G.J. Wilkie^a, W. Capecchi^b, S. Kubota^c, C. Hansen^{d,e}, V. Soukhanovskii^f

^a Princeton Plasma Physics Laboratory, Princeton, NJ, USA

^b Physics, University of Wisconsin, Madison, WI, USA

^c Physics and Astronomy, University of California, Los Angeles, CA, USA

^d Aeronautics and Astronautics, University of Washington, Seattle, WA, USA

^e Applied Physics and Applied Mathematics, Columbia University, New York, NY, USA

^f Lawrence Livermore National Laboratory, Livermore, CA, USA

ARTICLE INFO

Keywords:

Lithium wall
Plasma material interactions
Recycling

ABSTRACT

A comparison of three sets of Lithium Tokamak Experiment- β (LTX- β) discharges is presented, each with progressively more lithium evaporatively deposited on the stainless steel plasma facing components (PFCs). Multiple observations independently indicate a reduction in recycling with increasing lithium deposition - plasma current, discharge duration, density pumpout, and edge electron temperatures increase while plasma density and neutral influx decrease. These measurements make use of several new operational and diagnostics upgrades that have been installed on LTX- β to enable recycling analysis and quantification. Installation of an upgraded Supersonic Gas Injector (SGI) provides access to rapid density pumpout, enabling estimation of effective particle confinement times. Edge density and temperature are measured using a new, movable, low field side, off-midplane, swept single langmuir probe in addition to the LTX- β core Thomson scattering system. The neutral particle influx from the high field side limiter is measured using a hydrogen Lyman- α array. Prospects for future modeling and analysis integrating all of these measurements is discussed.

1. Introduction

In magnetic fusion devices, the neutral recycling coefficient R is defined as the ratio of the recycled neutral flux returning to the plasma from the PFCs Γ_{recy} to the flux of plasma ions incident on the plasma facing components Γ_{out} . Lithium is a low recycling material due to its ability to retain hydrogen from a plasma [1,2], and has been used in numerous devices for wall conditioning and density control [3–7]. It had long been theorized that a low recycling boundary will improve plasma performance by reducing the influx of cold neutral hydrogen into the plasma, thereby keeping the plasma edge hot [8]. Such an increase in plasma edge temperature and consequent reduction in temperature gradients from core to edge are expected to enable access to operating regimes with improved plasma confinement [9,10].

Flat electron temperature profiles, along with retention of hydrogen by lithium coated walls, were demonstrated in the Lithium Tokamak Experiment (LTX) [11]. However, the direct measurements of edge

neutral and plasma fluxes necessary to quantify the effects of recycling were not available for these experiments. The successor of LTX, LTX- β , is a spherical tokamak designed to systematically study the effect of a low recycling boundary on plasma performance in a tokamak [12,13]. Lithium coatings are evaporated onto an internal stainless-steel-clad copper shell conformal to the LTX- β plasma.

In this paper we present upgrades to LTX- β hardware and use them to investigate neutral and plasma density control in three identically programmed discharges, each with progressively more lithium on the PFCs. Section 2 is a brief description of the upgrades to the LTX- β lithium evaporators, supersonic gas injector, Langmuir probe, and poloidal Lyman- α array that were needed to make recycling analysis possible. Section 3 presents the effects of increasing lithium evaporation on plasma performance, density control, effective particle confinement τ_p^* , temperature profiles, and neutral influx from the wall. Finally, the implications for low recycling and future analysis are discussed in Section 4.

* Corresponding author.

E-mail address: amaan@pppl.gov (A. Maan).

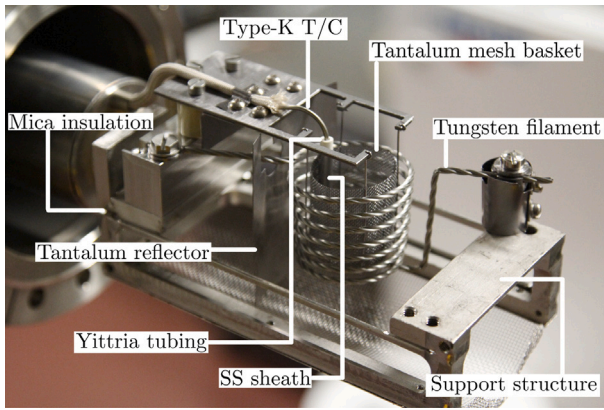


Fig. 1. LTX- β lithium evaporator, Mark-II. Chunks of lithium rod segments are placed inside the tantalum mesh, while the evaporator is under argon. The evaporator is then pumped to LTX- β relevant vacuum conditions before insertion into LTX- β at the center of the poloidal mid-plane. Once inserted, lithium inside the tantalum mesh basket is radiatively heated to evaporation temperatures, covering most of the first wall with a few tens, to a few hundred nm thick lithium coatings.

2. Operations and diagnostic upgrades for recycling studies

2.1. Improved coverage Mark-II lithium evaporators

Clean, rapid, and uniform lithium evaporation is an important technology necessary for the low-recycling regime. The previous version of LTX- β evaporators [13], referred to as Mark-I had some structural elements that blocked line of sight to the high field side of the PFC shells where the plasma typically limits. The blocking was resolved by re-designing the evaporator sub-assembly and minimizing structural elements that could cast a lithium shadow onto the high field side limiting PFCs. The evaporator sub-assembly (shown in Fig. 1) is mounted on a bellows drive that are stroked in to the poloidal center of the machine. Two evaporators are mounted diametrically opposite to each other. Mark-I evaporators were estimated to cover $\geq 86\%$ of the PFC [14], while the Mark-II evaporators cover an even larger fraction of the PFC. Mark-II evaporators have larger tantalum mesh basket that holds a charge of ~ 5 g per evaporator.

Once inserted fully, about ~ 60 A of current is run through a tungsten filament surrounding the basket, providing ~ 800 W of resistive heating. Radiation from the filament rapidly heats the lithium inside the tantalum basket to >500 °C. The temperature in the tantalum basket is monitored using a type-K thermocouple attached to it. Lithium deposition is monitored using Quartz Crystal Monitors (QCMs) mounted directly above the evaporator, with line of sight to the evaporator sub-assembly through a penetration in the PFC shell [14]. The evaporators can achieve a rapid lithium deposition rate of ~ 1 nm/sec. Typically a few tens of nanometers of lithium are deposited on LTX- β PFCs per evaporation at the beginning of a run day. Once lithium is evaporated on the PFCs, the evaporators are pulled back and plasma discharges are initiated.

LTX- β maintains a low base vacuum of $\sim 5 \times 10^{-8}$ Torr. A Residual Gas Analyzer (RGA) mounted on the vessel indicates water vapor is the largest Li-reactive vacuum contaminant at partial pressure of about an order of magnitude lower than base vacuum. Using the Hertz-Knudsen equation [15], we can estimate the impurity particle impingement rate on LTX- β PFC to be $\sim 5 \times 10^{15}$ / m^2s^{-1} . At an lithium evaporation rate of 1 nm/sec, we expect a lithium flux to the PFC of $\sim 1 \times 10^{17}$ / m^2s^{-1} , or two orders of magnitude greater than the flux of impurities to the surface. This implies LTX- β evaporators deposit a clean lithium film on the PFCs with close to 99% purity.

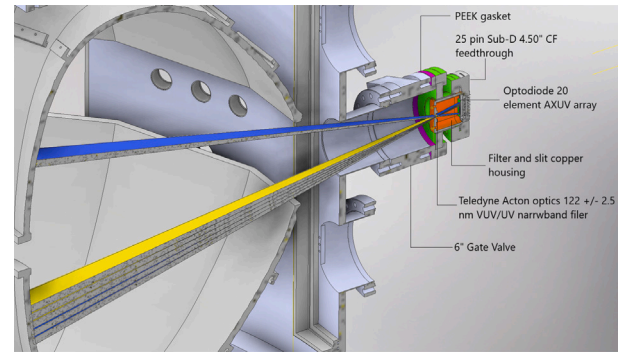


Fig. 2. CAD view of the Lyman- α array with various components.

2.2. Poloidal Lyman- α array

For fixed plasma parameters, hydrogen line emission is directly proportional to the neutral ionization rate, or alternatively the neutral density or the neutral flux. Hydrogen- α (656.3 nm) emission is frequently used as a proxy for recycling in magnetic fusion devices. However, lithium and its compounds have high reflectivity in the visible range [16] that can add spurious intensity from outside the field of view of the detector and confound analysis. Lithium has low reflectivity in the VUV range [17], and most of its compounds should as well [18]. Therefore, Lyman- α emission at 121.6 nm is expected to be a robust choice for recycling analysis.

The LTX- β Lyman- α array is depicted in Fig. 2. A 20 element AXUV photo-diode array is mounted vertically behind a 122 ± 2.5 nm VUV/UV narrow-band filter, housed in a light tight copper enclosure with a horizontal slit. The slit covers the filter such that each photo-diode samples a poloidal section of the high-field side limiting edge of the PFC shells as shown in Fig. 5(a). Line-integrated Lyman- α emission is calculated based on the manufacturer calibrated Lyman- α filter transmission, photo-diode responsivity and the engineering model of the array sightlines. The array pre-amplifiers were calibrated against a known bench top photo-diode amplifier by placing the array in a light-tight box, flashing an LED at the photo-diodes and recording the response separately using each gain setting on the pre-amplifier for every photodiode channel.

2.3. Supersonic gas injector (SGI)

Efficient, well-controlled plasma fueling is especially important when operating in the low recycling regime so as not to simply replace recycling with a similar low-efficiency, uncontrolled neutral source that also cools the edge [9,19]. The LTX- β SGI is based on a stainless steel Mach 5.5 nozzle attached to the outlet of a Veeco PV-10 gas valve, both retained from the LTX SGI [19]. Since the valve has a relatively modest temperature rating of ~ 50 °C, a double walled stainless steel heat shield was added around the valve body in anticipation of future hot shells operation at liquid lithium temperatures of >180 °C. A copper heat sink was also added to the re-entrant valve housing, with the air side cooled using a vortex tube. The LTX- β SGI is mounted vertically on a bellows drive and is driven into the vacuum vessel and through a penetration in the shell, such that the outlet of the SGI nozzle is flush with the PFC surface. This is done to ensure close coupling of the SGI to the plasma. Such a close coupling is important both for efficiency and for precise control of fueling response to the valve opening and closing.

2.4. Low field side scrape-off layer Langmuir probe

Measurement of scrape-off layer (SOL) plasma parameters and ion flux to the PFCs is necessary for understanding recycling and other

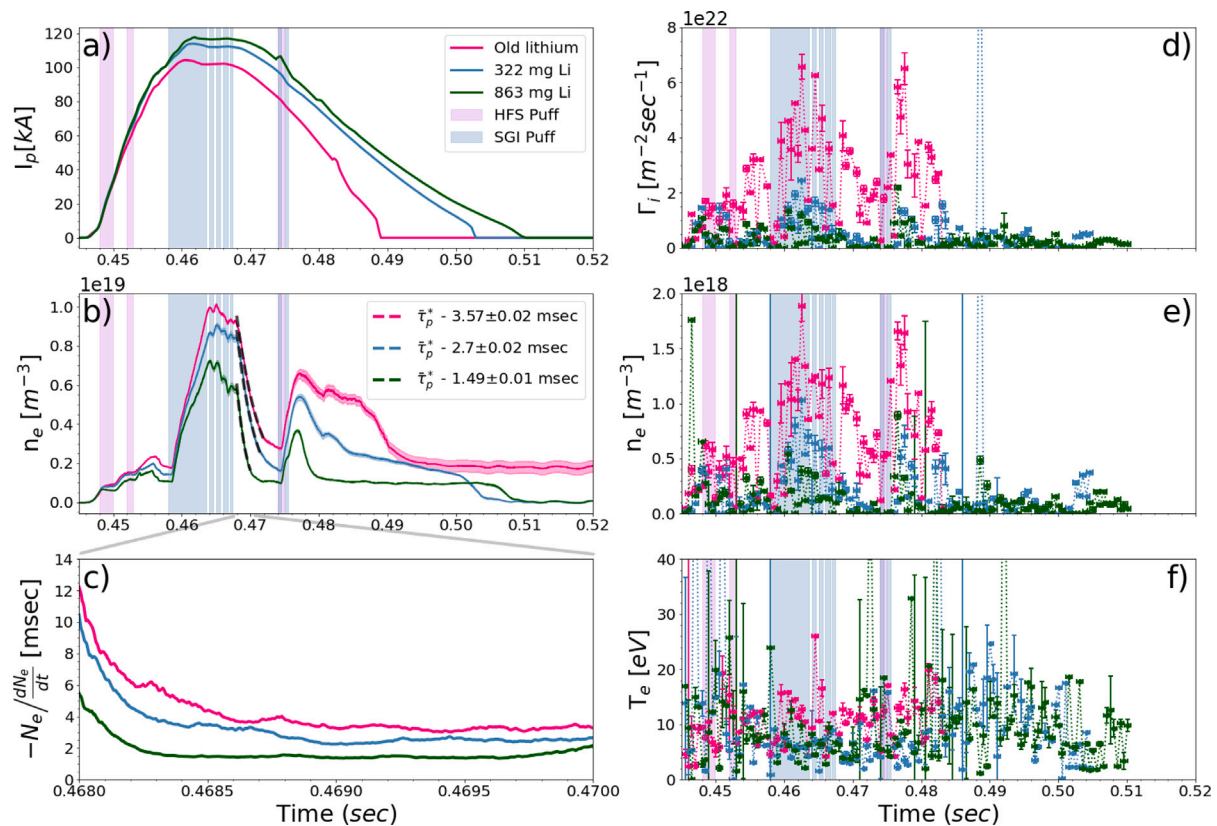


Fig. 3. (a) Plasma current for median shots and (b) Line averaged interferometer density waveforms averaged over all shots for the ensemble with 5-week-old lithium, 322 mg Li and 863 mg Li. Fueling is illustrated using vertical bands, exponential fits during density decay are illustrated by dashed lines and the corresponding decay constants for the three cases are listed in the legend. (c) $\tau_p^* = -N / \frac{dN}{dt}$ as a function of time during the density decay phase. (d) Ion flux measured by the LFS single langmuir probe, (e) electron density, and (f) electron temperature. The probe is 24.3 cm above midplane and the radial probe position was $R = 55.1$ cm, close to flush with the shells. Note the “Old lithium” density trace in (b) does not return to zero when the discharge terminates near 0.49 s; this is due to an uncorrected fringe jump after the second density peak and does not affect earlier data. Also note the zoomed in time axis for (c). (For interpretation of the references to color in this figure legend, the reader is referred to the web version of this article.)

plasma surface interactions, especially in the unique, collisionless, mirror trapped LTX- β SOL [20]. The new LTX- β low field side Langmuir probe is mounted on a bellows drive that allows the probe to be inserted radially up to 15 cm into the SOL through a gap between the PFC shell segments. In practice, however, the probe has not been inserted beyond 5 cm past the shells. The probe is installed 24.3 cm above the midplane in order to minimize interactions with runaway electrons that damaged the previous LTX- β Langmuir probe [21], likely during low density phases of the discharges [22]. The new probe was also designed using material with better temperature resistance and higher thermal mass. Boron nitride was used as the insulator instead of alumina while TZM, a molybdenum alloy was used for the sheath instead of stainless steel. Probe I-V traces are fit to a four parameter expression to account for sheath expansion that results in non-saturation of ion current evident in the probe data [23].

3. Reduced recycling experiments with increased lithium

3.1. Experimental setup

For this analysis we compare three sets of shots with identical coil and gas puff programming from different run days using progressively thicker lithium coatings. The initial “old lithium” shots were taken 5 weeks after the previous evaporation, enough time to mostly passivate the lithium coating deposited onto the PFCs [24,25]. For the 322 mg Li shot, lithium was evaporated at the beginning of the run day, average thickness of this Li coating is around 55 nm. Two lithium evaporation were performed for the 863 mg Li shot. The first evaporation was

performed at the beginning of the run day with an average lithium thickness of 105 nm. A subsequent evaporation with an average lithium coating thickness of ~ 57 nm was performed, midway through the run day.

As the same pre-programmed coil current and gas valve waveform were used for the different run days, maximum plasma current and shot duration are useful performance metrics for assessing wall conditions. Wall conditions are important for all fusion devices, as higher Z impurities and recycled neutrals increase density and cool the plasma, reducing conductivity. With increasing lithium coatings in LTX- β , shots are seen to last longer, have higher plasma current and reduced density. This improvement is well documented in earlier results [24,26]. Even as lithium coatings slowly oxidize, the performance gain persists even after days have passed since the last evaporation [14,25]. Only after the lithium coatings are several weeks old is a much stronger dip in plasma current and shot duration observed.

Each shot is repeated around 50 times per run day in order to collect Thomson scattering data at multiple time points, with a few shots per Thomson time point. Firing identical shots over the course of a run day also helps collect other diagnostic data that can be averaged together for improved statistics. Plasma current profile of the median shot is shown in 3 (a). Fringe-corrected line averaged density profiles of all the shots in an ensemble averaged together for three different run days is shown in Fig. 3 (b). The shots are primarily fueled using the SGI as can be seen from Fig. 3. The only other source of gas fueling in LTX- β is the High Field Side (HFS) puffer. The HFS puffer valve is situated outside the vacuum boundary. The outlet of the valve is attached to a tube with the other end between the toroidal shell gap on the high field

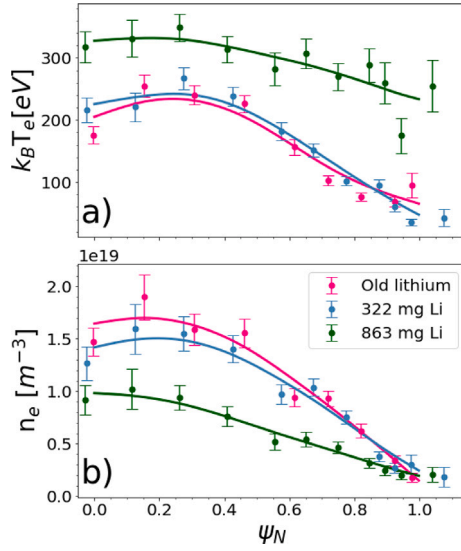


Fig. 4. (a) Core temperature and (b) density profiles in normalized flux coordinates at 468 ms, right after fueling and termination with passivated lithium, 322 mg Li and 863 mg Li as measured using LTX- β core Thomson scattering diagnostic, a smooth cubic spline fit is depicted using solid lines of respective colors. (For interpretation of the references to color in this figure legend, the reader is referred to the web version of this article.)

side. This means that even after the valve is shut down, the remaining gas in the tube dribbles into the plasma for several milliseconds. Such behavior effectively rules out the use of the HFS puffer for density decay time measurements.

3.2. Density control and particle confinement

The SGI has been successfully used in previous experiments [27] to measure the effective particle confinement times τ_p^* . Such a measurement can provide some insight into changes in recycling. For a tokamak plasma, if all external fueling sources are turned off, the plasma density decays exponentially; τ_p^* is the time constant of this decay [28]. Furthermore, τ_p^* is related to recycling by Eq. (4), where τ_p is the plasma particle confinement time. Implying that as recycling reduces, $\tau_p^* \rightarrow \tau_p$.

$$R \equiv \frac{\Gamma_{recy}}{\Gamma_{out}}, \quad \tau_p^* \approx \frac{N}{\Gamma_{out}} \quad (1)$$

$$\frac{dN}{dt} = \Gamma_{ext} + \Gamma_{recy} - \Gamma_{out} \approx \Gamma_{ext} - (1 - R) \frac{N}{\tau_p} \quad (2)$$

$$\text{for } \Gamma_{ext} \rightarrow 0, \quad N = N_0 \exp \frac{t}{\tau_p^*} \quad (3)$$

$$\tau_p^* = \frac{\tau_p}{1 - R} = - \frac{N}{\frac{dN}{dt}} \quad (4)$$

An average τ_p^* was estimated for the three discharges by fitting an exponential decay function during the density decay, Fig. 3(b), between 468 ms to 473 ms, over many shots and then taking an average. It was observed that τ_p^* reduces as more lithium is added to the machine, with the lowest $\tau_p^* = 1.5$ ms for 863 mg shots. Temporal evolution of τ_p^* is also tracked using Eq. (4), as shown in Fig. 3(c). It is observed that τ_p^* remains relatively flat during the density decay. For smaller ohmically heated tokamaks τ_p is expected to have a linear dependence on density [29]. However, the trend in the reduction of τ_p^* even when normalized to the peak averaged density persists, indicating that the reduction in τ_p^* is an indication of reduction in recycling.

Most conventional tokamaks use high recycling PFCs, with a global recycling coefficient anywhere between 0.9–1. At such high recycling

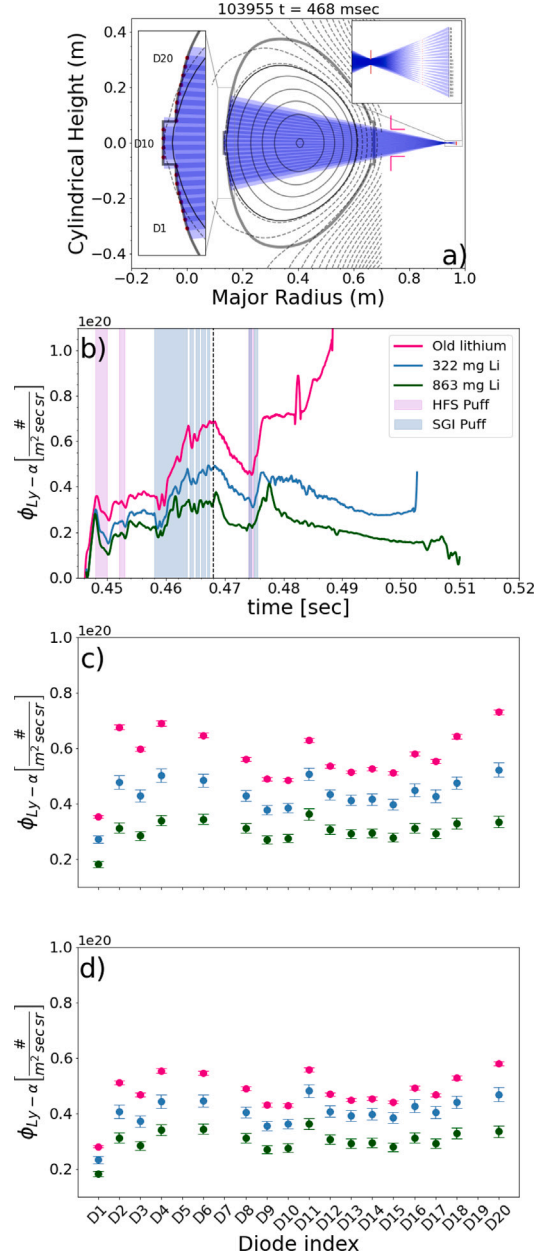


Fig. 5. (a) LTX- β Lyman- α array photo-diode sightline, poloidal view, (b) Lyman- α intensity as measured by the central diode aimed at the centerstack, the time stamp of interest (468 ms) is indicated by a vertical dashed line, gas puffs from the HFS puffer and the SGI are illustrated as in Fig. 3(c) Lyman- α signal across all photo-diodes in the array at 468 ms and (d) Lyman- α diodes at 469.9 ms for old lithium, 469.51 ms for 322 mg and 468 ms for 863 mg Li. (For interpretation of the references to color in this figure legend, the reader is referred to the web version of this article.)

τ_p^* can be anywhere between 10 to 100 times τ_p . However, that is likely not the case with LTX and LTX- β ; the demonstration of flat temperature profiles indicate that recycling is likely lower than those conventional values.

After the density from the initial set of large SGI puffs decays, the shots shown in Fig. 3 include a second, smaller set of puffs using both the SGI and HFS puffer to prevent density from dropping too low during the current ramp down. In the absence of the additional puffs, low density sometimes resulted in instabilities, disruptions, and/or runaway electrons. While no quantitative analysis of the second puffs has been attempted due to the more variable and rapidly changing behavior of

the plasma during ramp down, it is clear that the secondary density peaks and decay rates follow the same trends as the main SGI puffs.

3.3. Flat temperature profiles and low density SOL

Thomson scattering (TS) data was collected at multiple time points for these shots. Electron density and temperature profiles measured using the TS diagnostic was used to constrain kinetic equilibria for multiple time points per shot using PSI-TRI [30]. Across the three run days, shots evolve in an identical manner, they fill most of the volume at start-up and after 455 ms limit on the high field side. A typical reconstruction of these shots is depicted in Fig. 5(a). Solid contours in Fig. 5(a) represent region of confined plasma and dashed contours, inside the PFC shell structure, depicted by the gray colored solid boundary represent open field lines in the SOL. Each TS profile is averaged over a handful of shots to improve statistics. Fig. 4(a) shows the temperature profiles for the three run days at 468 ms, immediately after the SGI stops puffing in the gas. Notably the temperature profile with 863 mg lithium has relatively large temperature at the last closed flux surface (LCFS) and relatively low temperature gradient, a clear sign of the low recycling regime.

The langmuir probe is used to estimate ion flux, plasma density and temperature beyond the LCFS. Fig. 3(d), (e), (f) show probe data for the three cases where the probe was flush with the PFCs. The probe density is shown to track with the interferometer density as a function of time and lithiumization. However, there is no indication of increased plasma temperature for the 863 mg shot ensemble. This could be due to the inability of the probes to measure plasma temperatures beyond $\sim 30\text{eV}$. A new edge TS system is planned to better diagnose the SOL plasma for future campaigns.

Hot edge plasma temperatures, as seen in the TS data, has important implications for heat load at the strike points. Assuming the ion temperature is $> T_e/3$, the ion collisionality near the LCFS is low enough for a ion trapped fraction as high as 0.8 as estimated in TRANSP runs for these shot ensembles. As ion banana orbits immediately outside the LCFS are not collisionally destroyed, the plasma is expected to develop a potential along open field lines to retain electrons to maintain quasi-neutrality [20]. Such a hot collisionless SOL can increase the SOL power decay length λ_q by a factor of $\sim \sqrt{\frac{T_{\text{hot,LCFS}}}{T_{\text{cold,LCFS}}}}$ [31].

3.4. Reduced neutral influx

Lyman- α array was used to record the Lyman- α intensity along chords that view the high field side limiting surface. A consistent reduction in Lyman- α intensity is seen as more lithium is evaporated into the machine. As seen in Fig. 5(b), the central diode D11 (sightline shown in Fig. 5(a)) of the array shows a line integrated emission intensity that is the lowest for 863 mg Li. The Lyman- α intensity decay rate is the sharpest for 863 mg as well, indicating a quicker pumpout of hydrogen neutrals. Comparing the signal across the entire array at peak density (468 ms), also reveals a similar trend, where overall emission is the lowest for 863 mg Li and highest for the old lithium case, Fig. 5(c). Since Lyman- α intensity has a plasma density dependence, we also compare the measured Lyman- α intensity across all photo-diodes at time points of similar line averaged density. Fig. 5(d) depicts line integrated Lyman- α intensity measured by all diodes at 468 ms for 863 mg lithium, at 469.51 for 322 mg and at 469.9 ms for the old lithium case. Even for similar density the Lyman- α array shows a trend where the 863 mg shots have the lowest Lyman- α signal intensity, indicating reduced neutral density.

4. Discussion and conclusions

Various operational and diagnostic upgrades on LTX- β have made it possible to systematically study the effect of progressively adding more lithium to the tokamak's PFCs. By comparing discharges with different amounts of evaporated lithium, multiple independent observations indicate a reduction in fuel recycling with progressively more lithiumization. Plasma current and shot duration are shown to improve, temperature profiles are shown to flatten, Lyman- α intensity is shown to reduce as more lithium is evaporatively deposited on LTX- β PFCs. Improved density pumping as indicated by a reduction in peak density and τ_p^* is also observed with increased lithiumization.

To further quantify recycling, careful SOL analysis is needed for a realistic estimate of ion fluxes to the PFCs and interpretation of Lyman- α data. As indicated by the TS and probe data, at least the plasma immediately outside the LCFS, for the hot edge case is likely collisionless, which would need kinetic solvers to model. As a first step we are implementing 1x2v open field lines with LTX- β geometry in the full-f kinetic solver, GKEYLL [32]. The model should be able to quantify trapping along open field lines and estimate ion fluxes to the wall in a low collisionality SOL. The kinetic model for GKEYLL will then be used along with TS data to account for neutral particle population in these plasma using DEGAS2 [33]. A numerical recycling coefficient can be tuned in DEGAS2 to match the experimentally measured Lyman- α profiles, thereby estimating any change in recycling for these three cases.

CRediT authorship contribution statement

A. Maan: Conceptualization, Methodology, Software, Validation, Formal analysis, Investigation, Data curation, Writing – original draft, Writing – review & editing, Visualization. **D.P. Boyle:** Conceptualization, Methodology, Software, Validation, Formal analysis, Investigation, Data curation, Writing – original draft, Writing – review & editing, Visualization. **R. Majeski:** Conceptualization, Methodology, Formal analysis, Supervision, Project administration, Funding acquisition, Resources. **S. Banerjee:** Conceptualization, Methodology. **M. Francisquez:** Conceptualization, Methodology. **R. Kaita:** Conceptualization, Methodology, Formal analysis, Supervision, Project administration. **G.J. Wilkie:** Conceptualization, Methodology. **W. Capecchi:** Conceptualization, Methodology. **S. Kubota:** Software, Validation, Formal analysis, Investigation, Data curation. **C. Hansen:** Software, Validation, Formal analysis, Investigation, Data curation. **V. Soukhanovskii:** Validation, Investigation.

Declaration of competing interest

The authors declare the following financial interests/personal relationships which may be considered as potential competing interests: Anurag Maan reports financial support was provided by Princeton Plasma Physics Laboratory. Vlad Soukhanovskii reports financial support was provided by Lawrence Livermore National Laboratory. Chris Hansen reports financial support was provided by University of Washington.

Data availability

Data will be made available on request.

Acknowledgments

This work was supported by U.S. Department of Energy under contract numbers DE-AC02-09CH11466, DE-AC52-07NA27344, DE-SC0023481, and DE-SC0019239. The United States Government retains a non-exclusive, paid-up, irrevocable, world-wide license to publish or reproduce the published form of this manuscript, or allow others to do so, for United States Government purposes.

References

- [1] M. Baldwin, R. Doerner, S. Luckhardt, R. Conn, Deuterium retention in liquid lithium, *Nucl. Fusion* 42 (11) (2002) 1318, URL <http://stacks.iop.org/0029-5515/42/i=11/a=305>.
- [2] L. Buzi, Y. Yang, F. Dominguez-Gutierrez, A. Nelson, M. Hofman, P. Krstic, R. Kaita, B. Koel, Hydrogen retention in lithium and lithium oxide films, *J. Nucl. Mater.* 502 (2018) <http://dx.doi.org/10.1016/j.jnucmat.2018.02.010>.
- [3] J.S. Hu, Z. Sun, H.Y. Guo, J.G. Li, B.N. Wan, H.Q. Wang, S.Y. Ding, G.S. Xu, Y.F. Liang, D.K. Mansfield, R. Maingi, X.L. Zou, L. Wang, J. Ren, G.Z. Zuo, L. Zhang, Y.M. Duan, T.H. Shi, L.Q. Hu, E. team, New steady-state quiescent high-confinement plasma in an experimental advanced superconducting tokamak, *Phys. Rev. Lett.* 114 (2015) 055001, <http://dx.doi.org/10.1103/PhysRevLett.114.055001>, URL <https://link.aps.org/doi/10.1103/PhysRevLett.114.055001>.
- [4] R. Maingi, D. Boyle, J. Canik, S. Kaye, C. Skinner, J. Allain, M. Bell, R. Bell, S. Gerhardt, T. Gray, M. Jaworski, R. Kaita, H. Kugel, B. LeBlanc, J. Manickam, D. Mansfield, J. Menard, T. Osborne, R. Raman, A. Roquemore, S. Sabbagh, P. Snyder, V. Soukhanovskii, The effect of progressively increasing lithium coatings on plasma discharge characteristics, transport, edge profiles and ELM stability in the National Spherical Torus Experiment, *Nucl. Fusion* 52 (8) (2012) 083001, <http://dx.doi.org/10.1088/0029-5515/52/8/083001>.
- [5] D.K. Mansfield, K.W. Hill, J.D. Strachan, M.G. Bell, S.D. Scott, R. Budny, E.S. Marmar, J.A. Snipes, J.L. Terry, S. Batha, R.E. Bell, M. Bitter, C.E. Bush, Z. Chang, D.S. Darrow, D. Ernst, E. Fredrickson, B. Grek, H.W. Herrmann, A. Janos, D.L. Jassby, F.C. Jobses, D.W. Johnson, L.C. Johnson, F.M. Levintone, D.R. Mikkelsen, D. Mueller, D.K. Owens, H. Park, A.T. Ramsey, A.L. Roquemore, C.H. Skinner, T. Stevenson, B.C. Stratton, E. Synakowski, G. Taylor, A. von Halle, S. von Goeler, K.L. Wong, S.J. Zweben, Enhancement of Tokamak Fusion Test Reactor performance by lithium conditioning, *Phys. Plasmas* 3 (5) (1996) 1892–1897, <http://dx.doi.org/10.1063/1.871984>, arXiv:<https://doi.org/10.1063/1.871984>.
- [6] S.V. Mirnov, E.A. Azizov, V.A. Evtikhin, V.B. Lazarev, I.E. Lyublinski, A.V. Vertkov, D.Y. Prokhorov, Experiments with lithium limiter on T-11M tokamak and applications of the lithium capillary-pore system in future fusion reactor devices, *Plasma Phys. Control. Fusion* 48 (6) (2006) 821, <http://dx.doi.org/10.1088/0741-3335/48/6/009>.
- [7] M. Apicella, G. Mazzitelli, V. Pericoli Ridolfini, V. Lazarev, A. Alekseyev, A. Vertkov, R. Zagórski, First experiments with lithium limiter on FTU, *J. Nucl. Mater.* 363–365 (2007) 1346–1351, <http://dx.doi.org/10.1016/j.jnucmat.2007.01.237>, Plasma-Surface Interactions-17, URL <https://www.sciencedirect.com/science/article/pii/S0022311507002711>.
- [8] S.I. Krasheninnikov, L.E. Zakharov, G.V. Pereverzev, On lithium walls and the performance of magnetic fusion devices, *Phys. Plasmas* 10 (5) (2003) 1678–1682, <http://dx.doi.org/10.1063/1.1558293>, arXiv:<https://doi.org/10.1063/1.1558293>.
- [9] L. Zakharov, N. Gorelenkov, R. White, S. Krasheninnikov, G. Pereverzev, Ignited spherical tokamaks and plasma regimes with LiWalls, *Fusion Eng. Des.* 72 (1) (2004) 149–168, <http://dx.doi.org/10.1016/j.fusengdes.2004.07.015>, Special Issue on Innovative High-Power Density Concepts for Fusion Plasma Chambers, URL <http://www.sciencedirect.com/science/article/pii/S0920379604001140>.
- [10] P.J. Catto, R.D. Hazeltine, Isothermal tokamak, *Phys. Plasmas* 13 (12) (2006) 122508, <http://dx.doi.org/10.1063/1.2403090>, arXiv:<https://doi.org/10.1063/1.2403090>.
- [11] D.P. Boyle, R. Majeski, J.C. Schmitt, C. Hansen, R. Kaita, S. Kubota, M. Lucia, T.D. Rognlien, Observation of flat electron temperature profiles in the lithium tokamak experiment, *Phys. Rev. Lett.* 119 (2017) 015001, <http://dx.doi.org/10.1103/PhysRevLett.119.015001>, URL <https://link.aps.org/doi/10.1103/PhysRevLett.119.015001>.
- [12] J.C. Schmitt, R.E. Bell, D.P. Boyle, B. Esposti, R. Kaita, T. Kozub, B.P. LeBlanc, M. Lucia, R. Maingi, R. Majeski, E. Merino, S. Punjabi-Vinoth, G. Tchilingirian, A. Capece, B. Koel, J. Roszell, T.M. Biewer, T.K. Gray, S. Kubota, P. Beiersdorfer, K. Widmann, K. Tritz, High performance discharges in the Lithium Tokamak eXperiment with liquid lithium walls, *Phys. Plasmas* 22 (5) (2015) 056112, <http://dx.doi.org/10.1063/1.4921153>, arXiv:<https://aip.scitation.org/doi/pdf/10.1063/1.4921153>, URL <https://aip.scitation.org/doi/abs/10.1063/1.4921153>.
- [13] D. Elliott, J. Anderson, R.E. Bell, T.M. Biewer, D.P. Boyle, D. Donovan, C. Hansen, P. Hughes, R. Kaita, B. Koel, S. Kubota, R. Lunsford, A. Maan, R. Majeski, F. Scotti, V. Soukhanovskii, L. Zakharov, Initial results from the newly upgraded LTX- β , *IEEE Trans. Plasma Sci.* 48 (6) (2020) 1382–1387, <http://dx.doi.org/10.1109/TPS.2020.2983854>.
- [14] A. Maan, E. Ostrowski, R. Kaita, D. Donovan, R. Majeski, D. Boyle, P. Hughes, E. Merino, T. Kozub, B.E. Koel, D. Elliott, T. Biewer, F. Scotti, V. Soukhanovskii, R. Lunsford, Plasma facing component characterization and correlation with plasma conditions in lithium tokamak experiment- β , *IEEE Trans. Plasma Sci.* 48 (6) (2020) 1463–1467, <http://dx.doi.org/10.1109/TPS.2020.2969115>.
- [15] Thermodynamics and kinetics of adsorption and desorption, in: *Surface Science*, John Wiley & Sons, Ltd, pp. 185–228, <http://dx.doi.org/10.1002/9781119941798.ch4>, (Ch. 4), arXiv:<https://onlinelibrary.wiley.com/doi/pdf/10.1002/9781119941798.ch4>, URL <https://onlinelibrary.wiley.com/doi/abs/10.1002/9781119941798.ch4>.
- [16] E.M. Hollmann, A.Y. Pigarov, R.P. Doerner, Effect of graphite and molybdenum wall tile reflections on visible light diagnostics in tokamak experiments, *Rev. Sci. Instrum.* 74 (9) (2003) 3984–3990, <http://dx.doi.org/10.1063/1.1602941>, arXiv:<https://doi.org/10.1063/1.1602941>.
- [17] E. Palik, *Handbook of Optical Constants of Solids II*, Academic Press, Boston, 1991.
- [18] T.A. Callcott, E.T. Arakawa, Ultraviolet optical properties of li, *J. Opt. Soc. Amer.* 64 (6) (1974) 839–845, <http://dx.doi.org/10.1364/JOSA.64.000839>, URL <http://opg.optica.org/abstract.cfm?URI=josa-64-6-839>.
- [19] D.P. Lundberg, *Fueling Studies on the Lithium Tokamak Experiment* (Ph.D. thesis), Princeton University, 2012.
- [20] R. Majeski, R.E. Bell, D.P. Boyle, R. Kaita, T. Kozub, B.P. LeBlanc, M. Lucia, R. Maingi, E. Merino, Y. Raitses, J.C. Schmitt, J.P. Allain, F. Bedoya, J. Bialek, T.M. Biewer, J.M. Canik, L. Buzi, B.E. Koel, M.I. Patino, A.M. Capece, C. Hansen, T. Jarboe, S. Kubota, W.A. Peebles, K. Tritz, Compatibility of lithium plasma-facing surfaces with high edge temperatures in the Lithium Tokamak Experiment, *Phys. Plasmas* 24 (5) (2017) 056110, <http://dx.doi.org/10.1063/1.4977916>, arXiv:<https://doi.org/10.1063/1.4977916>.
- [21] A. Maan, *Lithium PFC Characterization and Plasma Performance for LTX- β* (Ph.D. thesis), University of Tennessee, 2020.
- [22] S. Munaretto, B. Chapman, B. Cornille, A. DuBois, K. McCollam, C. Sovinec, A. Almagri, J. Goetz, Generation and suppression of runaway electrons in MST tokamak plasmas, *Nucl. Fusion* 60 (4) (2020) 046024, <http://dx.doi.org/10.1088/1741-4326/ab73c0>.
- [23] D. Desideri, G. Serianni, Four parameter data fit for langmuir probes with nonsaturation of ion current, *Rev. Sci. Instrum.* 69 (6) (1998) 2354–2356, <http://dx.doi.org/10.1063/1.1148942>, arXiv:<https://doi.org/10.1063/1.1148942>.
- [24] R. Kaita, M. Lucia, J. Allain, F. Bedoya, R. Bell, D. Boyle, A. Capece, M. Jaworski, B. Koel, R. Majeski, J. Roszell, J. Schmitt, F. Scotti, C. Skinner, V. Soukhanovskii, Hydrogen retention in lithium on metallic walls from “in vacuo” analysis in LTX and implications for high-Z plasma-facing components in NSTX-U, *Fusion Eng. Des.* 117 (2017) 135–139, <http://dx.doi.org/10.1016/j.fusengdes.2016.06.056>, URL <http://www.sciencedirect.com/science/article/pii/S0920379616304574>.
- [25] A. Maan, D.P. Boyle, R. Kaita, E.T. Ostrowski, D.C. Donovan, R.P. Majeski, B.E. Koel, T.M. Biewer, P.E. Hughes, C. Hansen, S. Kubota, V. Soukhanovskii, Oxidation of lithium plasma facing components and its effect on plasma performance in the lithium tokamak experiment- β , *Plasma Phys. Control. Fusion* 63 (2) (2020) 025007, <http://dx.doi.org/10.1088/1361-6587/abcd0f>.
- [26] M. Lucia, R. Kaita, R. Majeski, F. Bedoya, J. Allain, T. Abrams, R. Bell, D. Boyle, M. Jaworski, J. Schmitt, Dependence of LTX plasma performance on surface conditions as determined by in situ analysis of plasma facing components, *J. Nucl. Mater.* 463 (2015) 907–910, <http://dx.doi.org/10.1016/j.jnucmat.2014.11.006>, URL <http://www.sciencedirect.com/science/article/pii/S0022311514007879>.
- [27] T. Gray, R. Kaita, R. Majeski, J. Spaleta, J. Timberlake, Fast gas injection as a diagnostic technique for particle confinement time measurements, *Rev. Sci. Instrum.* 77 (10) (2006) 10E901, <http://dx.doi.org/10.1063/1.2219379>, arXiv:<https://doi.org/10.1063/1.2219379>.
- [28] S.A. Cohen, Particle confinement and control in existing tokamaks, 1986.
- [29] S. Tsuji, Experimental scaling of particle confinement in tokamaks, *Fusion Eng. Des.* 15 (4) (1991) 311–324, [http://dx.doi.org/10.1016/0920-3796\(92\)90017-X](http://dx.doi.org/10.1016/0920-3796(92)90017-X), URL <https://www.sciencedirect.com/science/article/pii/S092037969290017X>.
- [30] C. Hansen, D.P. Boyle, J.C. Schmitt, R. Majeski, Equilibrium reconstruction with 3D eddy currents in the Lithium Tokamak eXperiment, *Phys. Plasmas* 24 (4) (2017) 042513, <http://dx.doi.org/10.1063/1.4981214>, arXiv:<https://doi.org/10.1063/1.4981214>.
- [31] A. de Castro, C. Moynihan, S. Stemmley, M. Szott, D.N. Ruzic, Lithium, a path to make fusion energy affordable, *Phys. Plasmas* 28 (5) (2021) 050901, <http://dx.doi.org/10.1063/5.0042437>, arXiv:<https://doi.org/10.1063/5.0042437>.
- [32] The Gkeyll team, The Gkeyll code, 2022, <http://gkeyll.readthedocs.io/>.
- [33] D. Stotler, C. Karney, Neutral Gas Transport Modeling with DEGAS 2, *Contrib. Plasma Phys.* 34 (2–3) (1994) 392–397, <http://dx.doi.org/10.1002/ctpp.2150340246>, URL <http://dx.doi.org/10.1002/ctpp.2150340246>.